SIMULATION TEST FOR A PUSH-TYPE PRECISION METERING DEVICE BASED ON DISCRETE ELEMENT METHOD

Lingyu Liu[1], Xiangcai Zhang[1*], Xiupei Cheng[1], Zhongcai Wei[1], Xianliang Wang[1]

[1*]Corresponding author. School of Agricultural Engineering and Food Science, Shandong University of Technology/Zibo, China.
E-mail address: zxcai0216@163.com | ORCID ID: https://orcid.org/0009-0003-9053-4398

ABSTRACT

To solve the problem of slow seed filling of soybean seeds under their own gravity, this study presents the design of a push-type precision metering device. Through a theoretical analysis, the key components and working principle of the push-type precision metering device were determined. The operational process was divided into two stages: dropping of seeds, and pushing of seeds. The discrete element method and a regression analysis were used to optimize the working parameters during the seed dropping stage. The optimal combination was found by the response surface optimization method, and both the seed dropping module and the whole machine were tested on a test bench with this parameter combination. The results showed that the optimal solution was obtained with a seed stirring disk speed of 17.57 r min⁻¹, 8.8 seed stirring rods (rounded to nine), and a central arc length proportion of 3.5% in the seed entry port. The predicted number of seeds dropped into the seed discharged cylinder (Y_1) under this parameter combination was 678.96, with a coefficient of variation of seed dropping uniformity (Y_2) of 6.33%. The experimental results gave values for Y_1 of 691.37 seeds and Y_2 of 6.93%, which were close to the predicted results.

INTRODUCTION

Precision planting (Wang et al., 2017a; Zhai et al., 2016) refers to an advanced technology that combines agronomic requirements for metering by accurately placing seeds into the soil at specified quantities, spacings, and depths. Precision planting not only saves seeds and reduces labor in regard to thinning seedlings, but also achieves uniform and robust seed emergence, laying a solid foundation for efficient production management while saving costs (Li et al., 2015; Liu et al., 2022). With the development of precision agriculture, the precise spatial distribution of seeds in three-dimensional coordinates has gradually become a research focus, with precision metering devices playing a crucial role in this process (Cong et al., 2014; Liu et al., 2019; Wang et al., 2017b).

Currently, precision metering devices (Ibrahim et al., 2018; Kus, 2021) are widely applied, and are of two main types, mechanical and pneumatic. Mechanical metering devices include horizontal disk (Teixeira et al., 2013), inclined disk (Correia et al., 2016), vertical disk, spoon, and clamp types (Xu et al., 2019), and are characterized by their simple structure, low processing costs, and stable operation. However, seeds are filled via gravity or mechanical clamping, leading to issues such as high rates of seed damage and slow filling speeds, making them unsuitable for high-speed planting operations. Current research efforts mainly focus on optimization through changes in hole shape and layout, the design of auxiliary filling methods (Zhang et al., 2022), or altering the discharging methods. Pneumatic metering devices include vacuum (Wang et al., 2023), air blow (Han et al., 2018), and integrated pneumatic types (Wang et al., 2022), in which pressure differentials are used for filling; this results in high filling speeds and low seed damage rates, making them suitable for high-speed precision planting. However, pneumatic metering devices have high requirements in terms of operating environments, as they requiring a continuous and stable pressure differential environment. They are prone to seed skipping issues, and are therefore unsuitable for operations in complex field environments and small plots.

In order to address the abovementioned issues, this study proposes a precision metering device and presents research on its structural design, working principle, and other

related aspects. Theoretical modeling, discrete element analysis and regression analysis are carried out to optimize the operational parameters of the seeding device at the seeding stage. Furthermore, experimental validation of the metering device's performance during the seed dropping stage and the overall operation of the machine is conducted using a test bench under the optimized operational parameters.

MATERIAL AND METHODS

Structure of the push-type precision metering device

The structural design of the precision metering device proposed in this study is illustrated in Figure 1, and consists primarily of a seed box, a seed stirring disk, a planetary gearbox, a transmission shaft, a housing, and a seed pushing device. The seed stirring disk has a conical shape, with stirring rods evenly distributed around its outer lower rim, while the inner wall of the housing contains eight seed entry ports and seed discharge cylinders. The seed pushing device is mainly composed of a seed pushing rod, seed pushing wheels, seed pushing modules, and spring hinges, where one end of the spring hinge is connected to the seed pushing module and the other is fixed to the outer surface of the housing. The seed stirring disk, planetary gearbox, seed pushing rod, and transmission shaft are interconnected and rotate co-axially counterclockwise.
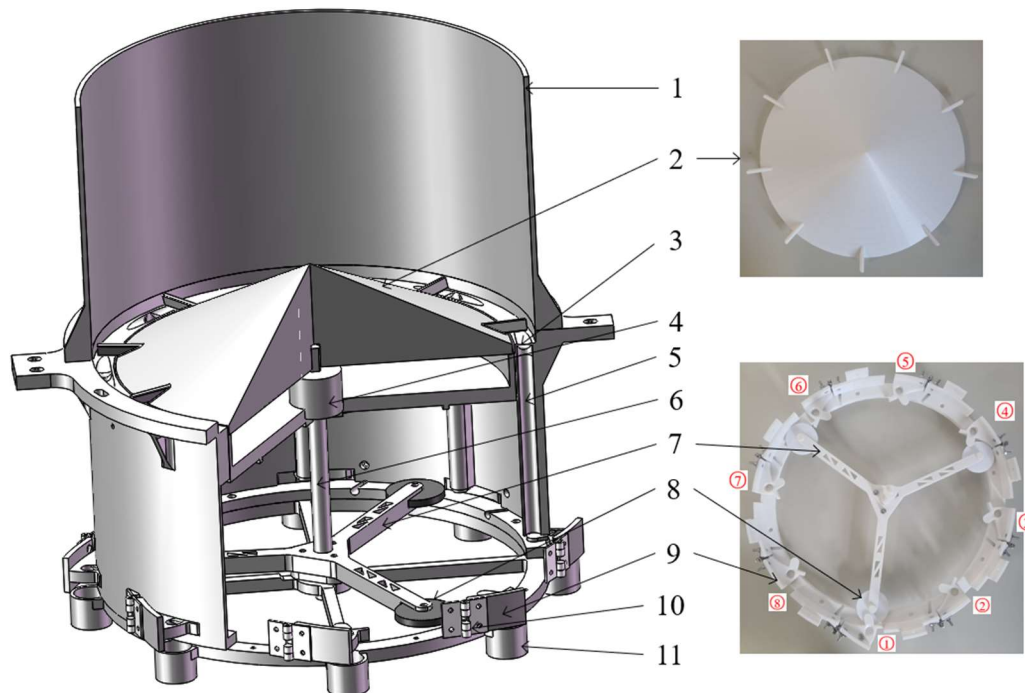
FIGURE 1. Structure of the precision metering device (1. seed box 2. seed stirring disk 3. seed entry port 4. planetary gearbox 5. seed discharge cylinder 6. transmission shaft 7. seed pushing rod 8. seed pushing wheel 9. seed pushing module 10. spring hinge 11. seed outlet)

Principle of operation of the precision metering device

The main characteristic of the metering device is its ability to achieve single-seed precision seeding for soybeans by altering the seeding method. In comparison to the gravity-based seeding method, where seeds are self-discharged, the seeds in the seed discharge cylinders are arranged vertically, thus exerting downward pressure on the seeds at the bottom and accelerating their entry into the seed pushing modules. The device is equipped with three seed pushing wheels and eight seed pushing modules, through which soybean seeds sequentially fall into eight seed outlets in the order 1-4-7-2-5-8-3-6. With each rotation of the transmission shaft, 24 seed pushes can be completed, allowing the seeds to be directed into the same row from different seed outlets based on the operational requirements, thereby facilitating single-row or multi-row planting.

The seeds are transferred in two stages: seed dropping and seed pushing. At the seed dropping stage, the transmission shaft is rotated counterclockwise under the power supplied from the external source, which drives the seed pushing rod and the input shaft of the planetary gearbox to rotate synchronously. After passing through the planetary gearbox, the rotational speed is reduced by a factor of 3.7. The output shaft of the planetary gearbox then drives the seed stirring disk to rotate coaxially. The soybean seeds in the seed box are randomly distributed near the seed entry port under the action of the conical surface of the seed stirring disk. As the seed stirring disk rotates, the seeds drop into the seed discharged cylinder and are arranged vertically. The soybean seeds at the bottom of the seed discharged cylinder are dropped into the seed pushing module and await pushing. To achieve seed pushing, the seed pushing wheel is installed at the outer end of the seed pushing rod. As this rod rotates, the seed pushing wheel rotates counterclockwise along the inner wall of the housing. When the wheel rotates to the seed pushing module, this module is pushed outward along the radial direction of the housing, simultaneously moving the soybean seeds within the module outward. The soybean seeds are then dropped into the seed outlet. After the seed pushing wheel has rotated, the seed pushing module returns to its

original position under the elastic force of the spring hinge, and the soybean seeds in the seed discharge cylinder drop into the seed pushing module again and await pushing, forming a periodic cycle.

Principle of operation of the seed dropping stage

At the seed dropping stage, the main task involves disturbing the seeds at the bottom of the seed box, causing them to fall from the seed entry port into the seed discharge cylinder and to be vertically arranged in the seed discharged cylinder, ready for the seed pushing stage. Soybean seeds in the seed box are randomly distributed near eight seed entry ports under the action of the conical surface of the seed stirring disk (with a conical angle of 30°, i.e., greater than the seed pile angle of 26.2°). The structure of the seed entry port is shown in Figure 2. When the seed stirring disk rotates, the seeds at the bottom of the seed box flow counterclockwise under the action of the rod. As the seeds flow towards the seed entry port, they gradually fall into the groove for seed entry. Under the combined action of the groove for seed entry guidance and the resultant force F_c, the seeds fall into the seed entry port (Shen et al., 2021). An analysis of the forces on the seeds along the radial surface of the housing is shown in Figure 3.
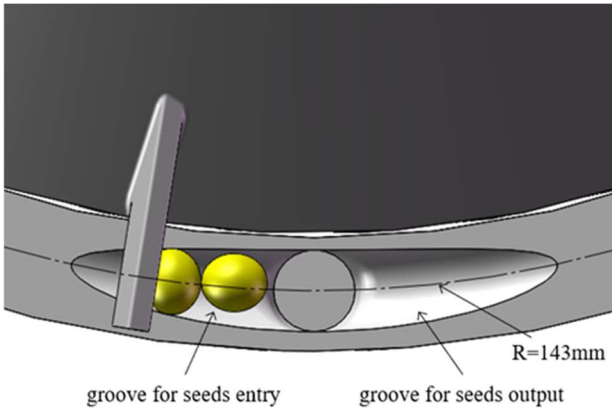
FIGURE 2. Top view of the seed entry port.
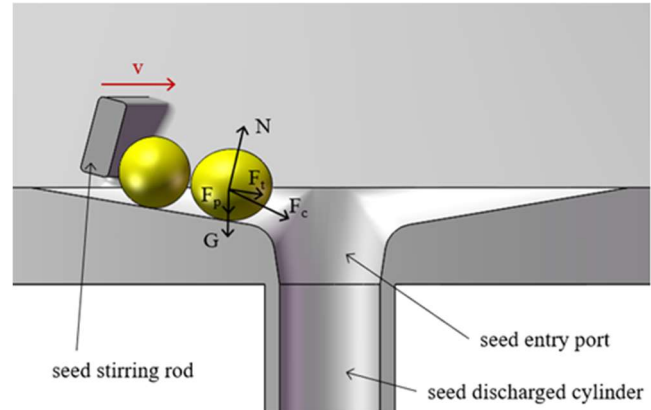
FIGURE 3. Forces on the seeds along the radial surface of the housing (neglecting friction)

$$F_c=N+F_t+F_p+G \tag{1}$$

Where:

N is the support force from the groove for seed entry on the seed;

F_t is the thrust from the seed stirring rod on the seed;

F_p is the population pressure on the seeds (variable direction), and

G is the gravitational force on the seed.

During this operation, the falling speed of the seed at the dropping stage is greater than the seed pushing speed at the pushing stage. After a certain period of time, the seeds will fill the eight seed discharge cylinders, and the seeds at the entry port will no longer continue to fall. Under the combined action of the stirring rod and the groove for seed output, the seeds are pushed out of the entry port, and an analysis of these forces is shown in Figure 4.
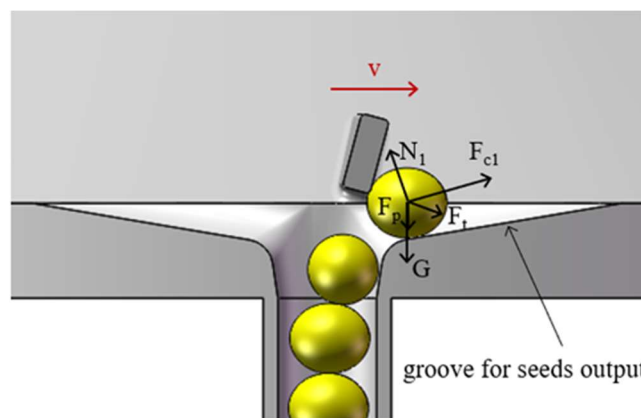
FIGURE 4. Diagram showing seeds pushed out by the force (neglecting friction).

$$F_{c1}=N_1+F_t+F_p+G \tag{2}$$

Where:

N₁ is the support force from the groove for seed output on the seed;

F_t is the thrust from the seed stirring rod on the seed;

F_p is the pressure on the seed (variable direction), and

G is the gravitational force on the seed.

Principle of operation of the seed pushing stage

At the seed pushing stage, the seeds inside the pushing module are propelled outwards and along with the movement of the pushing module, which causes them to enter the seed outlet, thus completing the pushing stage. At the dropping stage, the seeds are vertically arranged in the seed discharge cylinder, with the lower seeds falling into eight pushing modules at the bottom of the discharge cylinder under the influence of their own gravity and the pressure from the seeds above. Three seed pushing wheels rotate counterclockwise inside the housing, exerting pressure on the eight pushing modules to push them outwards sequentially, thereby facilitating the pushing stage of the seeds within the seed pushing modules. The pushing stage is illustrated in Figure 5.

To ensure that only one seed is expelled from each pushing module every time, and to avoid jamming of seeds at the pushing stage, a raising groove was designed in order to elevate the seeds waiting to be pushed. An analysis of the forces on the elevated seeds is illustrated in Figure 6.
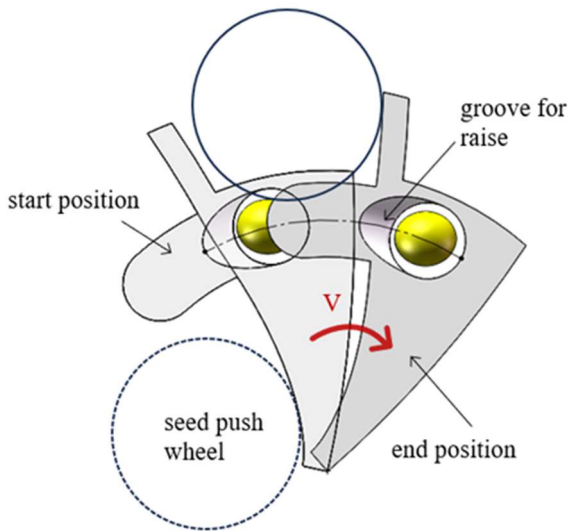
FIGURE 5. Schema of the pushing stage.
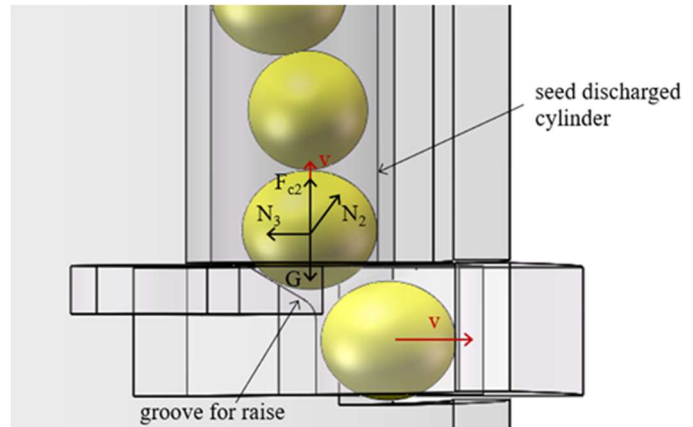
FIGURE 6. Analysis of forces on the elevated seed.

F_{c2} does not include the frictional force between the seed and the raising groove. The elevated seed is lifted upward in the direction of the resultant force F_{c2}. When the seed pushing module returns to its initial position, seeds continue to fall into the seed pushing module, awaiting the next pushing stage. F_{c2} is calculated as

$$F_{c2}=N_2+N_3+G \tag{3}$$

Where:

N₂ is the support force from the raising groove on the seed;

N₃ is the support force from the seed discharge cylinder on the seed, and

G is the gravitational force on the seed.

Diameter and parameters of the seed discharge cylinder

In order to familiarize ourselves with the size and morphology of soybean seeds, and as the basis for the design of the device (Dun et al., 2019), 100 randomly selected seeds of Zhonghuang 37 soybeans were measured using a digital caliper with an accuracy of ±0.02 mm. The dimensions of length (L), width (W), and height (H) of the soybean seeds were measured as shown in Figure 7.
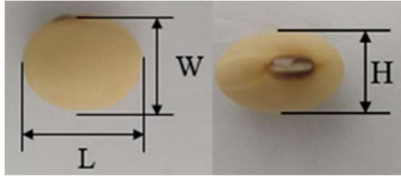
FIGURE 7. Schema showing the dimensions along the three axes of the seed

The average dimensions of the seeds were L=8.8 mm, W=7.3 mm, and H=6.1 mm. Over 93% of the seeds had a value of L<9.5 mm. In order to improve the seeding effect, seeds with a length greater than 9.5 mm were removed. The maximum seed diameter was therefore defined as D_{max}=9.5 mm. The diameter (Shen, 2021) of the seed discharge cylinder was set to

$$D=1.1 \times D_{max} \tag{4}$$

and the value of D was finalized at 10.4 mm.

Simulation parameters

Non-standard parts of this device were manufactured using 3D printing technology, with Somos8000 resin as the material of choice. In order to optimize the performance at the dropping stage, simulation experiments were conducted using the discrete element software EDEM (Park et al., 2021; Shi et al., 2022). The contact model employed was the Hertz-Mindlin non-slip contact model, with global variable parameters (Khatchatourian et al., 2014; Li et al., 2021; Chen, 2018) set as shown in Table 1.

TABLE 1. Global variable parameters.

Item	Parameters	Value
Soybean	Poisson's ratio	0.4
	Shear modulus / Pa	1.1×10^7
	Density / (kg m^{-3})	1111.3
Somos8000 resin	Poisson's ratio	0.35
	Shear modulus / Pa	1.2×10^8
	Density / (kg m^{-3})	1454.7
Soybean–soybean	Coefficient of restitution	0.41
	Coefficient of static friction	0.6
	Coefficient of rolling friction	0.044
Soybean–Somos8000 resin	Coefficient of restitution	0.32
	Coefficient of static friction	0.45
	Coefficient of rolling friction	0.04

Discrete modeling of soybean seeds

Based on the measurements along the three axial dimensions of soybean seeds, the equivalent seed diameter (Xue et al., 2019) D_s was calculated using [eq. (5)]:

$$D_s = \sqrt[3]{L \times W \times H} \tag{5}$$

Where:

L is the length of a soybean seed, mm;

W is the width, mm, and

H is the height, mm.

The average value of the seed equivalent diameter D_s after calculation was 7.3 mm, and [eq. (6)] was used to calculate the sphericity:

$$S_p = \frac{\overline{D_s}}{\overline{L}} \times 100\% \tag{6}$$

Where:

S_p is the sphericity of the soybean seed, %;

$\overline{D}$ is the average value of the seed equivalent diameter, mm, and

$\overline{L}$ is the mean value of the seed length, mm.

The sphericity of Zhonghuang 37 soybean seeds was calculated to be 83.4%, and four spherical objects were therefore employed to model the simulated particles, with dimensions of 8.8, 7.3, and 6.1 mm along the three axes, as shown in Figure 8.
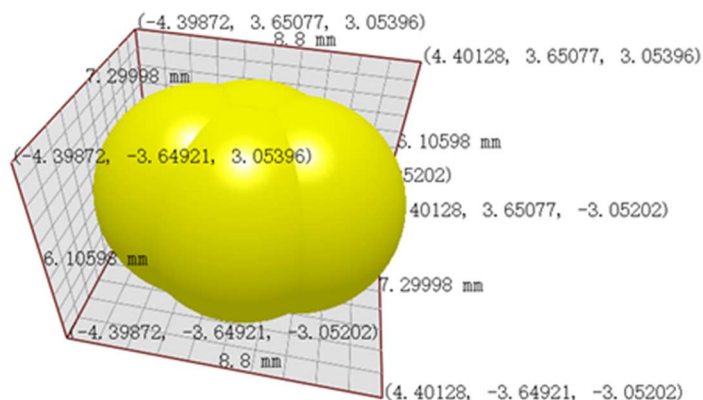
FIGURE 8. Modeling of a soybean seed.

Simulation model of the device

To facilitate calculations, the model of the push-type precision metering device was simplified to a seed box, a seed stirring disk (with conical surface and seed stirring rod), a housing (with seed entry ports and seed discharge cylinders), and seed pushing modules. A 3D model was drawn in Solidworks 2016, saved in STL format, and imported into EDEM software. Prior to the simulated planting process, 4000 seeds with a normal distribution were generated in the seed box. The simplified model of the push-type precision metering device is shown in Figure 9.
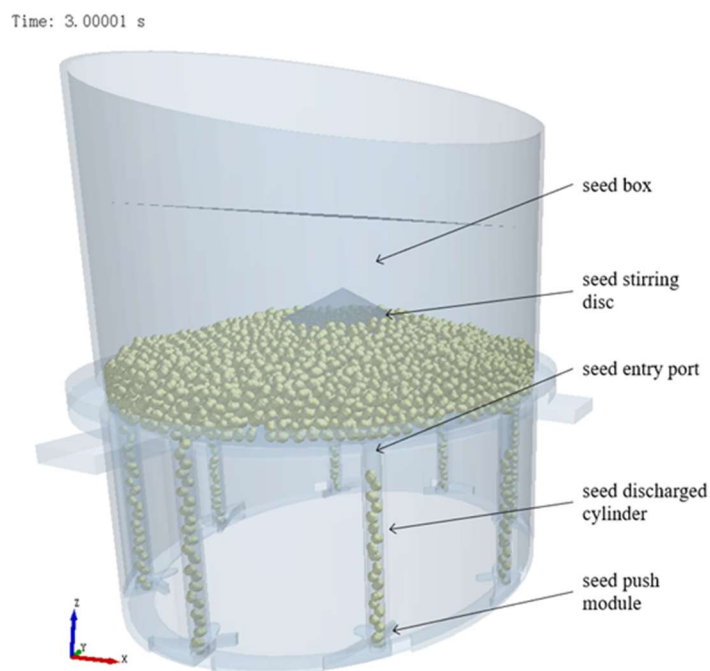
FIGURE 9. Simplified model of the push-type precision metering device.

Test method

In order to obtain an optimal combination of working dimensional parameters for the seed dropping stage, a three-factor simulation experiment involving the seed stirring disk speed (A), the number of seed stirring rods (B), and the central arc length proportion of the seed entry port (C) was conducted, in which single-factor experiments were integrated with structural dimension design. The experimental indicators were the number of seeds dropped in the seed discharge cylinder (Y_1) and the coefficient of variation in the seed dropping uniformity (Y_2). The Box-Behnken response surface optimization method was utilized for the three-factor, three-level simulation experiment to seek the optimal combination within constraint conditions and conduct verification, with each factor coded as shown in Table 2.

$$Y_1 = \sum_{i=1}^{n} x_i \tag{7}$$

Where:

x_i is the seed drop in the ith seed discharged cylinder, n=8.

$$Y_2 = \frac{\sqrt{\frac{1}{n-1} \sum_{i=1}^{n} (q_i - \bar{q})^2}}{\bar{q}} \tag{8}$$

Where:

$\bar{q}$ is the mean value of seed fall in the eight seed discharge cylinders, and

q_i is the seed drop in the ith seed discharged cylinder, n=8.

TABLE 2. Codes for each factor.

Codes	Factors		
	A (r min^{-1})	B (unit)	C (%)
1	7	6	1.5
2	14	8	2.5
3	21	10	3.5

Simulation setup and process

The simulation variable parameters used in EDEM are listed in Table 1. The seed box and housing were treated together, with each set simulation time being 10 s. The fixed time step was set to 15%, and the target save interval was set to 1×10^{-3} s. Linear rotational motion was applied to the central axis of the seed stirring disk, while sinusoidal rotational motion was applied to the push modules around the rotation axis. This setup allowed for observation of the soybean seeds entering the seed entry ports, with a grid bin group set up in the seed discharge cylinder to track the number of seeds that fell. In addition, the process of seeds leaving the seed entry port and being propelled by the push module could be observed.

Figure 10 illustrates the simulation process of seeds entering the seed entry port. In the Analyst interface, we replayed the simulation video, used manual selection to identify the target seed, and marked it in red. The seed marked in red could then be observed as it entered the seed entry groove, as shown in Figure 10(a), and eventually fell into the seed entry port, as shown in Figure 10(c), thus completing the seed dropping process.

(a)   (b)   (c)
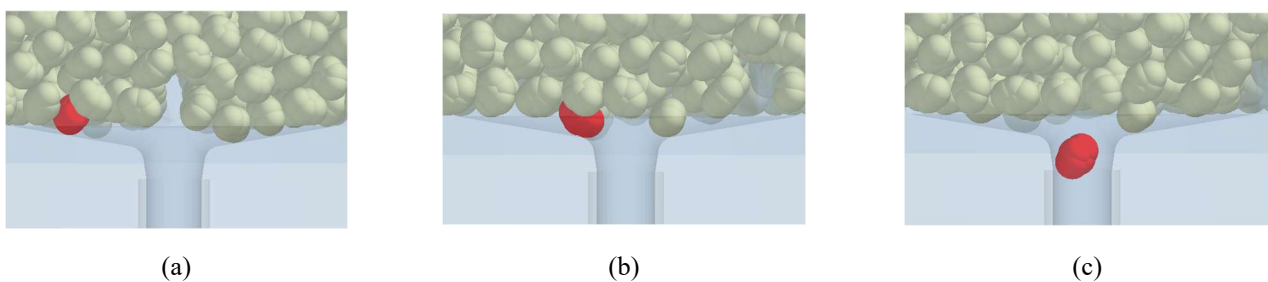
FIGURE 10. Simulation process of a seed entering the seed entry port

When the seed discharge cylinder is filled with seeds, the seeds at the seed entry port will be pushed out. Figure 11 shows the simulation process of seeds leaving the seed entry port. The marked seed can be observed over time: in Figure 11(a), it is pushed out from the seed entry port, and in Figure 11(c), it is pushed along the seed output groove and continues to flow in the seed box.

(a)   (b)   (c)
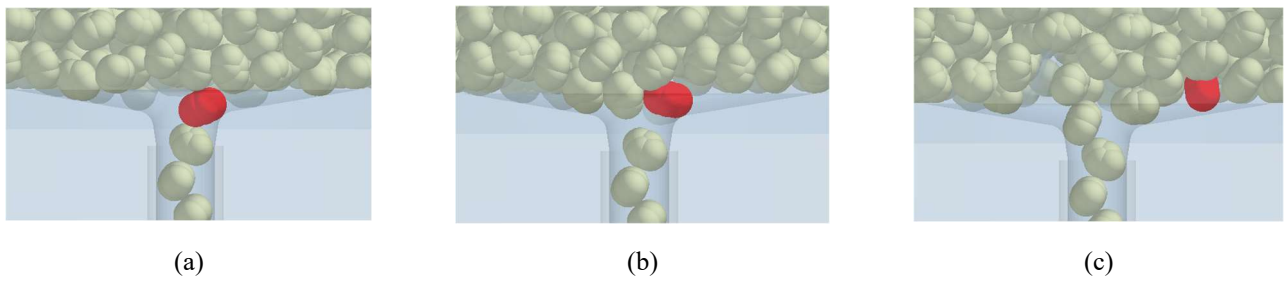
FIGURE 11. Simulation process of seeds leaving the seed entry port.

Under the pressure of the seeding wheel, the push modules are pushed outward; in the simulation, this action was replaced by sinusoidal rotational motion. Figure 12 illustrates the simulation process of seed pushing. The marked seed can be seen moving over time: in Figure 12(a), it is falling into the push module; in Figure 12(b), it is pushed out with the push module while lifting the next seed; and finally, in Figure 12(c), the seed leaves the push module and falls into the seed outlet, thus completing the pushing process.

(a)   (b)   (c)
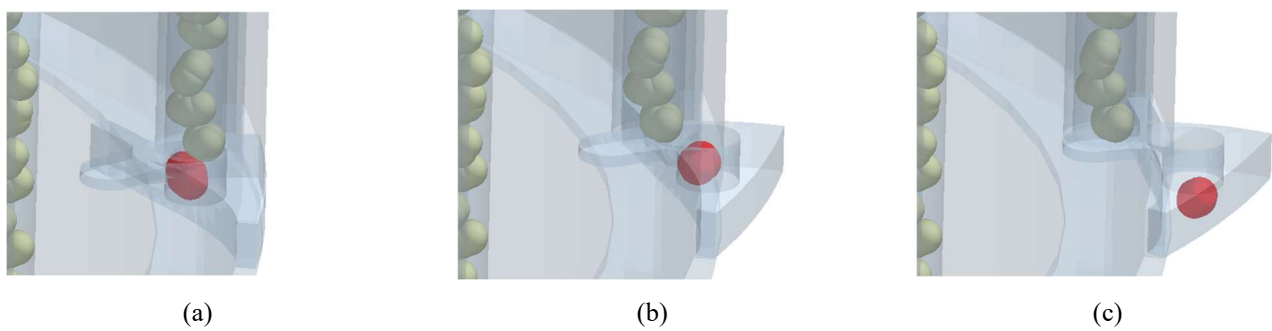
FIGURE 12. Simulation process of seed pushing

RESULTS AND DISCUSSION

The experimental results are presented in Table 3. Significance tests for the three experimental factors were conducted using Design-Expert software. By analyzing the evaluation indicators and regression coefficients obtained for the experimental factors, a second-order polynomial response regression model was established to describe their relationship. The model variance analysis and significance test results are shown in Table 4.

TABLE 3. Results of simulation experiments.

Number	Factors			Y_1 (unit)	Y_2 (%)
	A	B	C		
1	1	1	2	457	15.82
2	3	1	2	623	13.06
3	1	3	2	412	14.28
4	3	3	2	576	9.78
5	1	2	1	386	18.63
6	3	2	1	473	13.13
7	1	2	3	486	10.89
8	2	2	3	707	8.73
9	2	1	1	488	14.57
10	2	3	1	387	12.32
11	2	1	3	625	7.33
12	2	3	3	605	5.86
13	2	2	2	591	8.93
14	2	2	2	563	9.57
15	2	2	2	590	10.52
16	2	2	2	593	10.21
17	2	2	2	579	8.97

The results of the analysis of variance indicate that, for the number of seeds dropped in the seed discharged cylinder (Y_1), factors A, B, C, AC, BC, A^2, B^2, and C^2 had a highly significant impact, while the interaction AB was not significant. Regarding the coefficient of variation of seed dropping uniformity (Y_2), factors A, B, C, and A^2 had a highly significant impact, AC had a significant impact, and the interactions AB, BC, B^2, and C^2 were not significant.

TABLE 4. Results of a regression model variance analysis.

Variation source	Number of seeds dropped into the seed discharge cylinder (Y_1)				Coefficient of variation of seed dropping uniformity (Y_2)			
	Standard deviation square SS	df	F	P	Standard deviation square SS	df	F	P
Model	$1.37×10^5$	9	125.47	< 0.0001	168.95	9	51.88	< 0.0001
A	50880.5	1	419.24	< 0.0001	27.83	1	76.91	< 0.0001
B	5671012	1	46.73	0.0002	9.12	1	25.20	0.0015
C	59340.13	1	488.94	< 0.0001	83.46	1	230.68	< 0.0001
AB	1.0	1	$8.24×10^{-3}$	0.9302	0.76	1	2.09	0.1913
AC	4489.00	1	36.99	0.0005	2.79	1	7.71	0.0274
BC	1640.25	1	13.52	0.0079	0.15	1	0.42	0.5374
A^2	6644.53	1	54.75	0.0001	43.39	1	119.91	< 0.0001
B^2	2951.27	1	24.32	0.0017	0.62	1	1.72	0.2305
C^2	3910.42	1	32.22	0.0008	$1.05×10^{-4}$	1	$2.9×10^{-4}$	0.9869
Residual	849.55	7			2.53	7		
Lack of fit	220.75	3	0.47	0.7205	0.48	3	0.31	0.8196
Pure error	628.80	4			2.06	4		
Cor total	$1.379×10^5$	16			171.48	16		

In order to observe the impact of the interactions between various factors on the experimental indicators, one of the three experimental factors was held at a medium level and the others were varied. Response surface graphs (Figures 13 and 14) were created to visualize the results.

    a.   C=0.025   b.   B=8   c.   A=14r min⁻¹
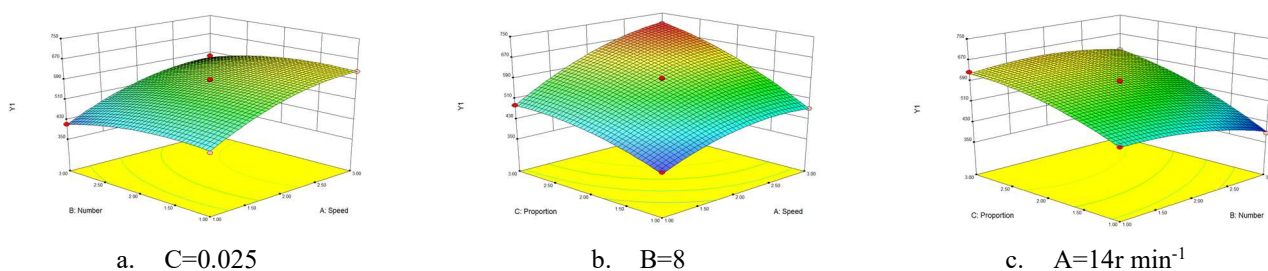
FIGURE 13. Effect of each test factor on Y_1 (predicted target value: 678.96).

    a.   C=0.025   b.   B=8   c.   A=14r min⁻¹
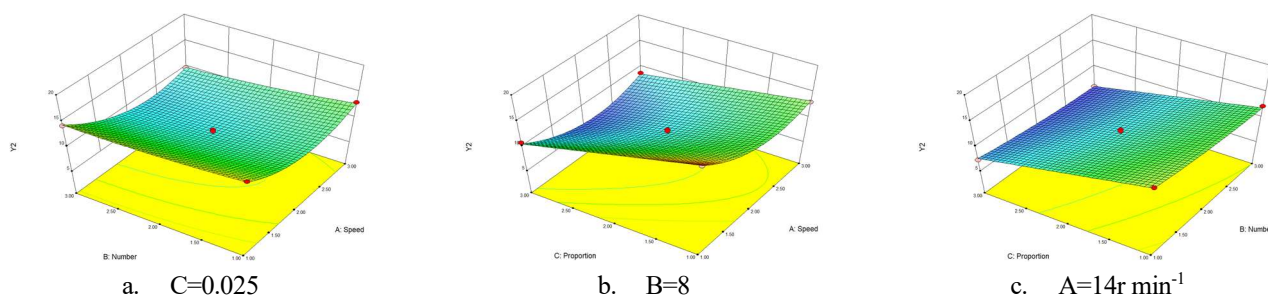
FIGURE 14. Effect of each test factor on Y_2 (predicted target value: 6.33%).

To find the optimal parameter combination under constraints, the following conditions were set: Y_1 should be greater than 800, and Y_2 should be less than 5%. Here, the importance percentage of Y_1 was set to 40%, while the importance percentage of Y_2 was set to 60%. An optimization analysis using Design-Expert software was conducted to solve the function.

$$\begin{cases} \max Y_1 \\ \min Y_2 \\ 7 \text{ r min}^{-1} \leq A \leq 21 \text{ r min}^{-1} \\ 6 \text{unit} \leq B \leq 10 \text{unit} \\ 1.5\% \leq C \leq 3.5\% \end{cases} \tag{9}$$

The optimal parameter combination was obtained as follows: the seed stirring disk speed was 17.57 r min^{-1}, the number of seed stirring rods was 8.8 (rounded to nine), and the central arc length proportion of the seed entry port was 3.5%. With this parameter combination, the predicted value of Y_1 was 678.96, and the predicted value of Y_2 was 6.33%.

The optimal combination of parameters was obtained based on the previous simulation experiments exploring the effect of the dropping stage structural parameters on the dropping performance. In order to test the performance of the dropping stage under this parameter combination and to determine whether it met the operational requirements of the seed pushing stage, a benchtop validation test of the push-type precision metering device was conducted. Furthermore, the reliability of the device was evaluated. The setup used for the benchtop test is illustrated in Figure 15.

FIGURE 15. Setup used for the benchtop validation test

The benchtop test was powered by a stepper motor, with eight cylinders placed below the seed outputs to receive the falling seeds. The test was repeated three times under the optimal combination of parameters. The average value of Y_1 at the dropping stage in the three tests was 691.37 seeds, and the average value of Y_2 was 6.93%, which were consistent with the predicted results. In the test phase, which included the pushing stage, the precision metering device pushed a total of 312 times, successfully pushing 299.68 seeds. The results indicate that under this combination of parameters, the dropping stage can effectively meet the working requirements of the pushing stage, and achieves good pushing performance for single soybean seeds, with stable reliability of the device.

CONCLUSIONS

(1) A push-type precision metering device was designed, which included two working stages: a seed dropping stage, and a seed pushing stage. This device was found to enable accurate individual seeding of soybean seeds, thereby laying a solid foundation for precision planting.

(2) Through the use of DEM simulation and regression analysis, the optimal combination of working parameters for the dropping stage was obtained. The results indicated a seed stirring disk speed of 17.57 r min^{-1}, a number of seed stirring rods of 8.8 (rounded to nine), and a central arc length proportion of the seed entry port of 3.5%. With this parameter combination, the predicted value of Y_1 was 678.96 seeds, and the predicted value of Y_2 was 6.33%. The test results gave values of Y_1 = 691.37 seeds and Y_2 = 6.93%.

(3) The pushing stage involves three pushing wheels and eight pushing modules. Each revolution of the transmission shaft can complete 24 pushes. During the sowing process, different seeds from various seed outlets can be directed to fall into the same row, according to the operational requirements, thereby facilitating single-row or multi-row planting.

REFERENCES

Cong JL, Yu JJ, Cao XY, Liao YT, Liao QG (2014) Design of Dual-purpose Pneumatic Precision Metering Device for Rape and Wheat. Transactions of the Chinese Society for Agricultural Machinery 45(1): 46-52. https://doi.org/10.6041/j.issn.1000-1298.2014.01.008

Correia TP Da S, Sousa SFG De, Silva PRA, Dias PP, Gomes ARA (2016) Sowing performance by a metering mechanism of continuous flow in different slope conditions. Engenharia Agrícola 36(5): 839-845. https://doi.org/10.1590/1809-4430-Eng.Agric.v36n5p839-845/2016

Chen YL (2018) Research of air-suction mechanical combined soybean high-speed and precision seed metering device. PhD Thesis, Jilin University, College of Biological and Agricultural Engineering.

Dun GQ, Yu CL, Yang YZ, Ye J, Du JX, Zhang JG (2019) Parameter simulation optimization and experiment of seed plate type hole for soybean breeding. Transactions of the Chinese Society of Agricultural Engineering 35(19): 62-73. https://doi.org/10.11975/j.issn.1002-6819.2019.19.008

Han DD, Zhang DG, Jing HR, Yang L, Cui T, Ding YQ, Wang ZD, Wang YX, Zhang TL (2018) DEM-CFD coupling simulation and optimization of an inside-filling air-blowing maize precision seed metering device. Computers and Electronics in Agriculture 7(150): 426-438. https://doi.org/10.1016/j.compag.2018.05.006

Ibrahim EJ, Liao QX, Wang L, Liao YT, Yao L (2018) Design and experiment of multi-row pneumatic precision metering device for rapeseed. International Journal of Agriculture and Biological Engineering 11(5): 116-123. http://dx.doi.org/10.25165/j.ijabe.20181105.3544

Khatchatourian OA, Binelo MO, de Lima RF (2014) Simulation of soya bean flow in mixed-flow dryers using DEM. Biosystems Engineering 123: 68-76. https://doi.org/10.1016/j.biosystemseng.2014.05.003

Kus E (2021) An attempt to evaluate the performance parameters of a precision vacuum seeder in different seed drop height. Journal of the Institute of Science and Technology 11(3): 1846-1853. http://dx.doi.org/10.21597/jist.930974

Li Y, He XT, Tao C, Zhang DX, Song S, Zhang R, Wang MT (2015) Development of mechatronic driving system for seed meters equipped on conventional precision corn planter. International Journal of Agricultural and Biological Engineering 8(4): 1-9. https://doi.org/10.25165/IJABE.V8I4.1717

Liu, CL, Wei D, Du X, Jiang M, Song JN, Zhang FY (2019) Design and test of wide seedling strip wheat precision hook-hole type seed-metering device. Transactions of the Chinese Society for Agricultural Machinery 50(1): 75-84. https://doi.org/10.6041/j.issn.1000-1298.2019.01.008

Li ZQ, Zhang P, Sun YC, Zheng CL, Xu L, E DY (2021) Discrete particle simulation of gas-solid flow in air-blowing seed metering device. Computer Modeling in Engineering and Sciences 127(3): 1119-1132. https://doi.org/10.32604/CMES.2021.016019

Liu CL, Li FL, Jiang M, Huang RB, Dai L, Gao ZP (2022) Design and experiment of the spotting glue-paper tape precision seeder for small seed vegetables. Transactions of the Chinese Society of Agricultural Engineering 38(13): 20-29. https://doi.org/10.11975/j.issn.1002-6819.2022.13.003

Park D, Lee CG, Yang D, Kim JY, Rhee JY (2021) Analysis of inter-particle contact parameters of garlic cloves using discrete element method. Journal of Biosystems Engineering 46(4): 332-345. https://doi.org/10.1007/s42853-021-00110-0

Shen H, Zhang JJ, Chen XH, Dong JX, Huang YX, Shi JT (2021) Development of a guiding-groove precision metering device for high-speed planting of soybean. Transactions of the ASABE 64(3): 1113-1122. https://doi.org/10.13031/trans.14307

Shen H (2021) Development of a guiding-groove precision metering device for high speed planting of soybean. Master Thesis, Northwest A&F University, College of Mechanical and Electronic Engineering. https://doi.org/10.27409/d.cnki.gxbnu.2021.000943

Shi LR, Yang XP, Zhao WY, Sun BG, Wang N, Sun W (2022) Effect of potato contact parameters on seed metering performance using discrete element method. Spanish Journal of Agricultural Research 20(1): 1-15. http://dx.doi.org/10.5424/sjar/2022201-18499

Teixeira SS, dos Reis AV, Machado ALT (2013) Longitudinal distribution of bean seeds in horizontal plate meter operating with one or two seed outlets. Engenharia Agrícola 33(3): 569-574. https://doi.org/10.1590/s0100-69162013000300013

Wang JW, Tang H, Wang JF, Shen HG, Feng X, Huang HN (2017a) Analysis and experiment of guiding and dropping migratory mechanism on pickup finger precision seed metering device for corn. Transactions of the Chinese Society for Agricultural Machinery 48(1): 29-37+46. https://doi.org/10.6041/j.issn.1000-1298.2017.01.005

Wang JW, Tang H, Wang JF, Li X, Huang HN (2017b) Optimization design and experiment on ripple surface type pickup finger of precision maize seed metering device. International Journal of Agriculture and Biological Engineering 10(1): 61-71. https://doi.org/10.3965/j.ijabe.20171001.2050

Wang YC, Le YD, Luo SB, Sun H, Chen HT (2022) Design and experiment of centralized precision soybean seed-metering device. Transactions of the Chinese Society for Agricultural Machinery 49(6): 112-118. https://doi.org/10.6041/j.issn.1000-1298.2018.06.013

Wang C, Yang HY, He J, Kang KX, Li HW (2023) The influence of seed variety and high seeding speed on pneumatic precision seed metering. Engenharia Agrícola 43(3): e20220183. https://doi.org/10.1590/1809-4430-eng.agric.v43n3e20220183/2023

Xu J, Cai ZS, Zhang GS, Shen P (2019) Simulation optimization of declined disc scoop type soybean seed metering device based on discrete element method. Journal of Agricultural Mechanization Research 41(5): 8-15. https://doi.org/10.13427/j.cnki.njyi.2019.05.002

Xue P, Xia XY, Gao PY, Ren D, Hao YJ, Zheng ZQ, Zhang JC, Zhu RX, Hu B, Huang YX (2019) Double-setting seed-metering device for precision planting of soybean at high speeds. Transactions of the ASABE 62(1): 187-196. https://doi.org/10.13031/trans.13055

Zhai JB, Xia JF, Zhou Y (2016) Design and experiment of pneumatic precision hill-drop drilling seed metering device for hybrid rice. Transactions of the Chinese Society for Agricultural Machinery 47(1): 75-82. https://doi.org/10.6041/j.issn.1000-1298.2016.01.011

Zhang XJ, Cheng JP, Shi ZG, Zhang YL, Wang MJ (2022) Design and experiment of a clamp-holding precision maize-seed-metering device. Engenharia Agrícola 42(6): e20220049. https://doi.org/10.1590/1809-4430-eng.agric.v42n6e20220049/2022